Neutrons in coincidence with fission of ^{238}U induced by stopped antiprotons

W. Schmid, T. von Egidy, F. J. Hartmann, J. Hoffmann, and S. Schmid
Physik-Department, Technische Universität München, D-85748 Garching, Germany

D. Hilscher, D. Polster, and H. Rossner
Hahn-Meitner-Institut-Berlin, D-14109 Berlin, Germany

A. S. Iljinov, M. V. Mebel, D. I. Ivanov, V. G. Nedorezov, and A. S. Sudov
Institute for Nuclear Research, Russian Academy of Science, 117312 Moscow, Russia

H. Machner and H. S. Plendl*
KFA Jülich, D-52425 Jülich, Germany

J. Eades and S. Neumaier
CERN, 1211-Geneva 21, Switzerland
(Received 23 December 1996)

Neutron multiplicities after antiproton-induced fission have been determined as a function of the total mass of the fission fragments. Pre- and postscission neutron multiplicities of the reaction $\bar{p}+^{238}$U have been deduced using the moving-source parametrization of the neutron energy spectra by Maxwellian distributions. A postscission multiplicity of 6.3(6) neutrons out of 20.0(10) in total emitted neutrons in fission indicates that fission is a rather slow process. The increase of the evaporative prescission neutron multiplicity is about 80% of the total increase of evaporative neutrons as a measure of excitation energy. The postscission multiplicity gets only 20% of the total increase, thus indicating that the nucleus has only a moderate excitation energy at the moment of scission. The results are compared with standard cascade-evaporation calculations predicting a much lower number of evaporated prescission neutrons as the experiment shows. This is a strong indication of the importance of dissipative effects in the fission process. Application of dissipative effects like a saddle-to-scission delay time and nuclear viscosity in the model calculation describes the experimental results much better. [S0556-2813(97)04806-1]

PACS number(s): 25.43.+t, 25.70.Gh, 25.85.Ge

I. INTRODUCTION

Nuclear reactions induced by stopped antiprotons deserve special interest because of their unique mechanism of producing hot nuclei with excitation energies up to 800 MeV and at the same time transferring only moderate angular momentum to the nucleus. Compared to high-energy heavy-ion reactions only slight compression of the nuclear matter occurs. In the case of nuclear fission two of the interesting questions are the descent from saddle to scission and how fission is influenced by dissipative effects. Even after more than 50 years research in fission the saddle to scission transition of a nucleus is not completely understood. Especially the measurement of pre- and postscission particles, mainly neutrons, gives insight into the competition between particle emission and fission and valuable information of the dynamics of fission. Defining a time scale by neutron evaporation gives a possibility to answer the following question: ''How fast is fission?''

II. EXPERIMENTAL METHOD

The experiment was carried out at the LEAR storage ring of CERN. The experimental arrangement consisting of fission-fragment and neutron counters is depicted in Fig. 1. A low-energy antiproton-beam ($\bar{p}$) with a momentum of 200 MeV/c entered the fission chamber through thin (thickness 100 μm) Beryllium and Mylar (thickness 36 μm) windows, went through a plastic scintillation counter telescope

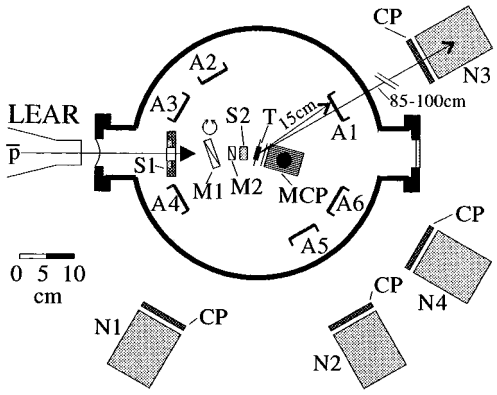

FIG. 1. Horizontal section through the setup of the experiment at LEAR. $A1-A6$ are pin-diode arrays, $N1-N4$ neutron counters, CP veto counters for charged particles, $S1$,$S2$ the antiproton scintillator telescope, $M1$,$M2$ variable degraders, T the target, and MCP a microchannel plate.

*Permanent address: Physics Department, Florida State University, Tallahassee, FL 32306.

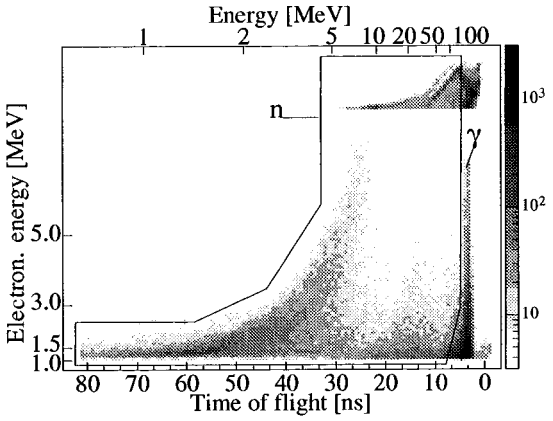

FIG. 2. Selection of neutrons (n) and γ rays (γ) in the energy (pulse-height) vs TOF scatterplot. The energy on the ordinate is derived from the pulse-height signal; the energy on the abscissa is calculated from TOF. The upper part shows the energy derived from the PM-Dynode 11 signal used to increase the maximum detectable energy to about 100 MeV; for the lower part the signal from dynode 14 was used, resulting an energy interval from the threshold energy (see Table I) of about 1 MeV up to 10 MeV. The boot-shaped region (n) marks the neutron events.

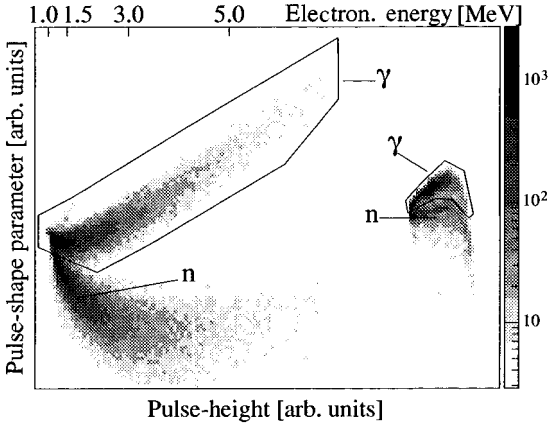

FIG. 3. Selection of neutrons (n) and γ rays (γ) in the pulse shape vs energy (pulse height) plot. Note that the energy on the abscissa is the energy derived from the pulse-height signal (ordinate from Fig. 2). The pulse-shape parameter is explained in the text. The right part was obtained using the signal from dynode 11. The regions denoted with (γ) contain the discarded γ events.

($S1$,$S2$) and was brought to rest in the uranium target (T) by means of plastic degraders ($M1$,$M2$). The target was a self-supporting foil of uranium of natural isotope composition with a thickness of 2.3 mg/cm^2 and a diameter of 15 mm.

The walls of the fission chamber were of steel with a thickness of 4 mm in order to be transparent for neutrons. Six pin-diode arrays (A1–A6) were used as fission-fragment detectors, each consisting of 6 × 12 single counters with an area of 1 cm^2. They measured energy, time-of-flight (TOF), direction and angular correlation of the fission fragments. The direction measurement is possible by the coincidence of one of the 12 time signals from the rows of the array with one of the 6 energy signals coming from a column of the pin-diode arrays. Details about the pin-diode array detectors and their properties as fission-fragment detectors are described by Kim *et al.* [1]. The start signal for the TOF measurement is given by a microchannel-plate detector (MCP) counting the electrons ejected by the fission fragments emerging from the target. The electrons were deflected by 90° into the micro-channel-plate by an electrostatical mirror, thus making it possible to detect strongly ionizing particles, like fission fragments, producing many delta electrons. The neutrons were registered at four angles (0°, 30°, 60°, and 90°) with respect to the fission axis by NE213 liquid scintillation counters ($N1$–$N4$). The detectors measured TOF, energy (pulse-height) and a pulse-shape signal in order to discriminate γ rays from neutrons. In addition plastic-scintillator veto counters (CP) (thickness 3 mm) in front of the neutron counters ($N1$–$N4$) were used to reject charged particles. Neutrons or, to be more precise, recoil protons from the neutrons were selected by the time-of-flight vs energy relation (Fig. 2) and the pulse-shape vs energy plot (Fig. 3). The discrimination of neutrons from γ's in Fig. 3 exploits the different decay times of radiative states in the scintillation material NE213 corresponding to different ionization-densities of recoil protons and electrons corresponding to γ rays. The pulse-shape parameter in Fig. 3 is the difference between two integrations over the scintillation light pulse with a short and a long integration time [2]. The efficiency of the neutron counters was calculated with the help of the Monte Carlo program of Cecil *et al.* [3] which also takes into account all the inelastic reaction channels with the carbon nuclei of the organic scintillator liquid. The properties of the neutron detectors are listed in Table I. As one can see from the setup of Fig. 1, there were 12 possibilities for the emission angle of neutrons to be combined from four neutron counters and three pairs of fission counters. Due to the symmetry of the setup each angle occured three times for different neutron detectors. This reduces systematic errors caused by detector-specific thresholds and efficiencies in neutron detection remarkably.

For the energy and time-of-flight measurements of the fission fragments with the pin-diode detectors corrections for the pulse-height defect (PHD) and the plasma-delay effects, respectively, were taken into account. These corrections, however, depend both already on the mass of the measured particle one just wants to determine. For the pulse-height defect a correction formula by Schmitt *et al.* [4] was used; the plasma delay was corrected following an expression given by Neidel *et al.* [5]. Some of the parameters in the formulas of Schmitt and Neidel are specific for the type of the detector and were determined in previous test measurements [1] with fission fragments from ^{252}Cf(sf) and ^{235}U($n_{\rm th}$,f). An iterative procedure was applied to determine

TABLE I. Some properties of the neutron counters. The threshold energy for neutrons was determined by the Compton edge of ^{22}Na. The time resolution was 1.2 ns (FWHM).

Detector	Threshold MeV	Target distance cm	Diameter cm	Thickness cm
$N1$	0.96	95.2	12.3	10.2
$N2$	0.94	82.4	10.2	10.2
$N3$	0.96	92.0	12.3	10.2
$N4$	0.78	99.5	12.3	10.2

the corrections for time-of-flight and energy simultaneously. Some complications for the pulse-height-defect correction with the Schmitt formula come from the wide range of fission-fragment energies caused by different emission angles and energy losses in the target. Especially in the low-energy region the PHD corrections became too high and a method which reduces the correction smoothly for low fragment energies was developed [6,7].

As a third correction the energy loss of the fission fragments in the target was calculated with stopping-power values taken from the heavy-ion range-energy tables of Northcliffe and Schilling [8]. The emission angle of the fragments with respect to the target plane was taken into account. In first order the sum of the path lengths of the fragments within the target does not depend on the depth where fission takes place, but only on the emission angle. The energy loss for crossing half the target thickness varied from 12 MeV to 22 MeV for emission angles with the target surface varying between 90° and 30°. Therefore the energy-loss correction for the total kinetic energy (TKE) of both fragments can be made more precise as it is the case for the kinetic energy of a single fragment, where the path length and energy loss in the target material is unknown.

The trigger condition MT for the readout of the electronics was

$$\mathrm{MT}=\overline{S1}*S2*(A1+\cdots+A6). \tag{1}$$

Here $\overline{S1}*S2$ denotes the signal from a $\overline{p}$ passing through the scintillator $S2$ without hitting the ring-counter $S1$, and $(A1+\cdots+A6)$ means at least one pin-diode signal from any of the pin-diode arrays $A1$–$A6$. TOF, energy and the other parameters of the four neutron counters and the energy information of the pin diodes were then read out. A more elaborate fission trigger for the neutron detectors was made off line by software cuts in the TOF-energy relation of the pin-diode measurements. Two different triggers were applied in the software analysis, one by demanding only one fission fragment for inclusive neutron spectra, and a more restrictive one demanding both fragments in coincidence for a precise definition of the fission axis for the exclusive neutron spectra. The fission fragments (FF) were identified by their time-of-flight vs energy relation which is depicted in Fig. 4. Particles with masses from 60 to 160 u and energies from 12 to 160 MeV were associated with fission fragments.

III. DATA TREATMENT

Though the angular and energy dependence of the neutron emission gives the information about pre- and post scission particles it is also interesting to study in addition the inclusive energy spectrum of neutrons from fission. In the case of isotropic emission the inclusive measurement means no loss of information. The use of a less restrictive trigger condition for fission leads to an increase of the statistics, which is important for the high-energy region. In particular this trigger condition was the registration of only one fission fragment. The inclusive energy spectrum of the fission-coincident neutrons is shown in Fig. 5. This spectrum was fitted by a sum of three distributions [9]:

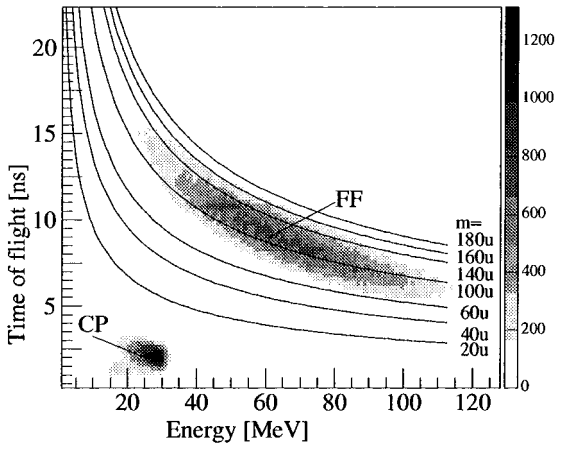

FIG. 4. TOF vs energy plot for fission fragments (FF) and charged particles (CP). The solid lines are isobars for different masses. The pulse-height defect was corrected only for $m>45$ u.

$$\frac{dM}{dE}=\sum_{i=1}^{3}\frac{2M_i\sqrt{E}}{\pi^{1/2}T_i^{3/2}}\exp\left(-\frac{E}{T_i}\right). \tag{2}$$

M_i and T_i are the multiplicities and temperature parameters for source i. E is the energy of the neutrons. The energy range of the fit extended from 3 MeV to 150 MeV. The results of the fit varying all the M_i and T_i is compiled in Table II. The statistical error was determined by a 10% change of the reduced χ^2, as it was done by the authors of [13]. The errors given in all the following tables are the statistical and the systematic error. For multiplicities a systematic error of 8% resulting from the accuracy of the Monte Carlo efficiency calculation was assumed.

Looking at Fig. 5 one can easily identify two components in the spectrum, a high-energy part which can be ascribed to the emission of neutrons during the intranuclear cascade (INC) and a low-energy component resulting from the evaporation of both the compound nucleus (CN) and the fission fragments (FF). For properly describing the data it was

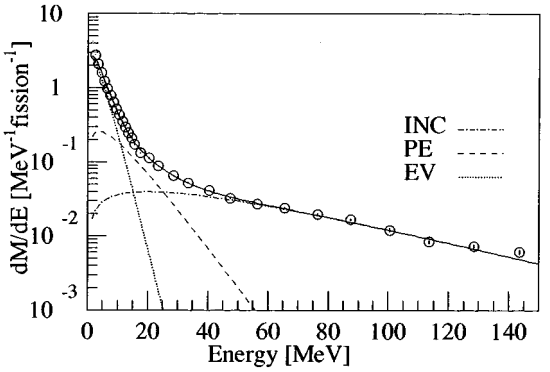

FIG. 5. Inclusive energy spectrum of neutrons in $\bar{p}$-induced fission of ^{238}U. All events with at least one fission fragment in coincidence were collected. The curves (dotted) are the components of the fit. INC means intranuclear cascade, PE preequilibrium, and EV evaporation. The sum of the components is drawn as a solid line.

TABLE II. Multiplicities M and temperatures T from a three source fit to the neutron spectra of $^{238}U(\bar{p},f)$. The error given in brackets is the quadratic sum of the statistical and the systematic errors.

M_{INC}	3.33(30)	Neutrons
M_{PE}	3.95(32)	Neutrons
M_{EV}	13.2(11)	Neutrons
T_{INC}	40.1(34)	MeV
T_{PE}	7.54(45)	MeV
T_{EV}	2.55(16)	MeV

necessary to introduce a third source which can be interpreted as the preequilibrium emission (PE) after the fast cascade has finished and before the nucleus has attained thermal equilibrium. Attempts to fit with only two sources resulted in a considerably worse value of χ^2. Also it cannot be expected that after the emission of the highly energetic cascade neutrons the emission continues with the low-energy evaporation neutrons.

The principle of the measurement of pre- and postscission neutrons was invented by Harding and Farley [10]. It relies on the fact that the emission of neutrons from the moving fission fragments is strongly enhanced in the direction of the fission axis while perpendicular to the fission axis the count rate is lower. Moreover, the energy spectrum of the fission neutrons is changed depending on the direction in which the neutrons are registered. The emission of neutrons before scission from the compound nucleus is isotropic if the compound nucleus is at rest in the laboratory frame. As the antiproton annihilation of stopped antiprotons occurs via formation of an antiprotonic atom the only means of transferring momentum to the compound nucleus is by the pions produced in the annihilation. Measurements of this momentum transfer in $\bar{p}$ on ^{238}U have shown that it is small compared to the velocity of the fission fragments, justifying the assumption of a compound nucleus at rest; the measured mean momentum of the fragments is 722 ± 10 MeV/c [11] which converts to an energy per nucleon of only 6×10^{-3}MeV/nucleon. This is two order of magnitudes smaller than the mean energy per nucleon in the fragments. For the fission fragments a mean energy per nucleon of 0.698 MeV/nucleon was assumed and taken as a fixed input parameter for the fit. It was derived from the TKE value of 152.2 MeV and the total mass of 211.6 u measured by Hofmann *et al.* [11] for the $\bar{p}$-induced fission of ^{238}U. This mass,

TABLE III. Neutron multiplicities M and temperatures T as a result of a moving source fit according to Eq. (3) to the energy spectra. T_{INC} and T_{PE} were held fixed at the values of Table II.

M_{INC}	3.3(3)	Neutrons
M_{PE}	4.1(4)	Neutrons
M_{CN}	6.2(6)	Neutrons
$M_{FF1,2}$	3.2(3)	Neutrons
T_{CN}	2.58(21)	MeV
$T_{FF1,2}$	1.90(18)	MeV
T_{INC}	40.1 (fixed)	MeV
T_{PE}	7.54 (fixed)	MeV

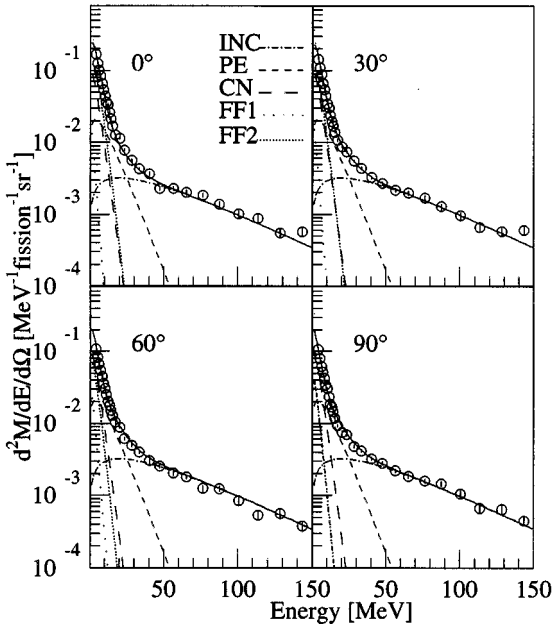

FIG. 6. Neutron energy spectra for $^{238}U(\bar{p},f)$ for emission angles of 0°, 30°, 60°, and 90° with respect to the fission axis. The curves (dotted, dashed, and dash-dotted) are the components of the moving source fit functions. The solid line is the sum of the components.

of course, is measured after emission of the postscission neutrons and charged particles. Adding as a rough estimate the number of 6.3 postscission neutrons, one gets 218 u for the mass of the scissioning nucleus, resulting in a mean energy of 0.698 MeV/nucleon.

To decompose the neutron spectra into the pre- and postscission multiplicities a moving-source parametrization

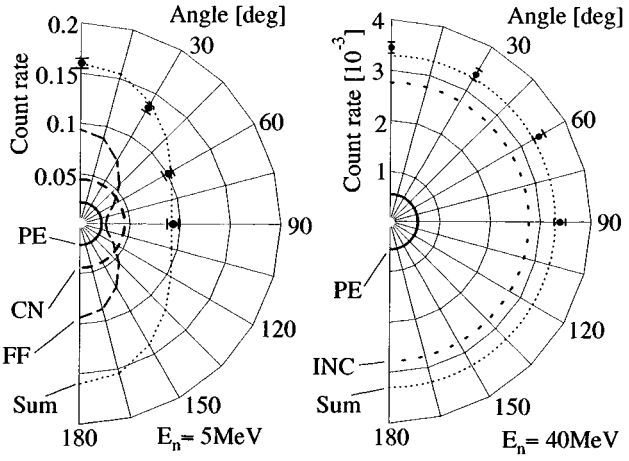

FIG. 7. The curves are the fitted distributions and their sum given by Eq. (3) and the results in Table IV. Only the statistical errors are displayed. The fission axis is in the direction 0° and 180°. The pictures show the emission characteristics for neutrons with energies of 5 MeV (left) and 40 MeV (right). Emission characteristics from the compound-nucleus evaporation (CN), from the fission fragment neutrons (FF), the preequilibrium emission (PE), and from the intranuclear cascade (INC) are indicated.

TABLE IV. Anisotropy of neutron emission given by the ratio of count rates $W(0°)/W(90°)$ for selected neutron energies. $W(0°)$ and $W(90°)$ are also displayed in Fig. 7.

Energy	$W(0°)/W(90°)$	
MeV	Experiment	Fit acc. to Eq. (3)
5	1.84(3)	1.76
40	1.02(7)	1.00
1.5–150	1.386(11)	1.384

was applied. The neutron spectra were fitted by Maxwellian spectra [9] with isotropic emission in the emitter frame. In the laboratory system the emission is then explicitly given by

$$\frac{d^2M}{dEd\Omega}=\sum_{i=1}^{5}\frac{M_i\sqrt{E}}{2(\pi T_i)^{3/2}}\exp\left(-\frac{E-2\sqrt{\varepsilon_i E}\cos\Psi_i+\varepsilon_i}{T_i}\right). \tag{3}$$

Here M_i and T_i denote the multiplicity and temperature parameters for source i, respectively, ε_i is the mean energy per nucleon of source i, Ψ_i the angle between the direction of movement of the source i and the detector viewing the emitted neutrons. The spectra were fitted in an energy region ranging from 3 MeV to 150 MeV. The temperature parameters $T_{\rm INC}$ and $T_{\rm PE}$ were held fixed at the values obtained in the inclusive fit. The other parameters T_i and M_i were varied. The results are given in Table III. The functions fitted according to Eq. (3) are depicted, together with the measured energy spectra, in Fig. 6. The measured and calculated angular distributions (cf. Fig. 7) clearly show that the assumption of isotropically emitted neutrons is fulfilled during the intranuclear cascade (see Table IV). The multiplicities for the INC and PE components agree well with the inclusive data. The total multiplicity of 20.0(10) neutrons is equal within the error bars to 20.4(12) neutrons from the inclusive measurement.

The excitation energy of the thermalized hot nuclei can be estimated from the measured mass of both coincident fission fragments. The mass loss which is roughly proportional to the excitation energy is given by the difference of the target mass and the mass of both fragments. The fission-coincident neutrons were sorted according to four regions of the total fragment mass or mass loss. The resulting neutron spectra are described for each mass-loss region given in Table V with the moving-source parametrization defined by Eq. (3). The temperature parameters for the intranuclear cascade and preequilibrium component were fixed at the values of Table III.

The prescission multiplicity of neutrons $M_{\rm pre}$ is defined as the sum of the multiplicities $M_{\rm INC}$, $M_{\rm PE}$, and $M_{\rm CN}$:

$$M_{\rm pre}=M_{\rm INC}+M_{\rm PE}+M_{\rm CN}. \tag{4}$$

The postscission multiplicity is simply the sum of the two neutron numbers $M_{\rm FF1}$ and $M_{\rm FF2}$ evaporated by the fission fragments:

$$M_{\rm post}=M_{\rm FF1}+M_{\rm FF2}=2M_{\rm FF1,2}. \tag{5}$$

Table V shows the result for the different windows. The number of postscission neutrons depends only slightly on the mass loss, whereas the number of prescission neutrons increases strongly with increasing mass loss. Due to the poor mass resolution of the setup (29 u FWHM) a correction had to be applied on the pre- and postscission multiplicities of Table V. From the mass resolution a correlation matrix for the four mass loss windows was calculated. The correlation matrix [7] describes the probability of a certain mass value to be found in the wrong mass window. Of course, the measured values in Table V have statistical fluctuations as they are experimental data. The unfolding of the measured values with the correlation matrix leads to an increase in these errors. For this reason a linearization of the measured values in Table V was applied before the unfolding procedure was performed. A consequence of this treatment is a linear dependence of the resulting multiplicity values from the mass loss or mass as they are shown in Table VI or open data points as in Fig. 8. We observe that about half of the measured mass loss is due to neutron emission while the rest must be due to charged particles which we did not measure in this experiment.

IV. COMPARISON WITH OTHER EXPERIMENTS AND METHODS

Comparing the present exclusive results with the inclusive experiment of Polster *et al.* [14] (see Table VII) one finds

TABLE V. Compilation of neutron multiplicities M and temperature parameters T for different mass loss windows. The last column shows the values averaged over all masses. The number $M_{\rm pre}$ of prescission neutrons is the sum of the neutron numbers $M_{\rm INC}$, $M_{\rm PE}$, and $M_{\rm CN}$. The number $M_{\rm post}$ of postscission neutrons is defined as $2*M_{\rm FF1,2}$.

Mass loss [u]	>45	30–45	15–30	<15	All masses
$M_{\rm INC}$	4.1(6)	3.7(4)	2.5(5)	2.5(4)	3.2
$M_{\rm PE}$	4.8(7)	4.4(5)	3.5(4)	2.1(4)	3.7
$M_{\rm CN}$	8.2(10)	6.3(7)	6.1(7)	5.6(7)	6.6
$M_{\rm FF1,2}$	3.1(4)	3.5(4)	3.0(4)	2.9(3)	3.1
$M_{\rm pre}$	17.1(14)	14.4(10)	12.2(10)	10.2(9)	13,5
$M_{\rm post}$	6.3(6)	7.0(8)	6.0(7)	5.8(7)	6.3
M_{Σ}	23.4(15)	21.4(13)	18.2(12)	16.0(11)	19.8
$T_{\rm FF1,2}$ [MeV]	2.0(3)	2.0(3)	1.8(2)	1.6(2)	1.9
$T_{\rm CN}$ [MeV]	3.0(3)	2.6(3)	2.3(2)	3.1(3)	2.8

TABLE VI. Neutron multiplicities M as a function of mass loss. The same as Table V, but corrected for the mass resolution in the fission-fragment measurement.

Mass loss [u]	>45	30–45	15–30	<15
M_{INC}	4.6(6)	3.6(5)	2.8(5)	1.8(4)
M_{PE}	5.8(7)	4.4(5)	3.1(4)	1.6(3)
M_{CN}	8.4(10)	7.1(7)	6.0(7)	4.7(7)
$M_{FF1,2}$	3.4(4)	3.2(4)	3.1(4)	2.9(3)
M_{pre}	18.8(14)	15.1(10)	11.9(10)	8.1(9)
M_{post}	6.8(6)	6.4(8)	6.2(7)	5.8(7)
M_{Σ}	25.6(15)	21.5(13)	18.1(12)	13.9(11)

good agreement for the multiplicity and mean energy of the INC and CN components. In these data, too, there is a component describing the pre-equilibrium emission with similar mean energy but with a remarkably lower multiplicity of only 1.15 neutrons. Looking at the total multiplicity one finds 18.1(14) neutrons in the experiment of Polster *et al.* and 16.3(9) in the measurement of Chen *et al.* [15] compared to the 20.4(12) neutrons from our experiment.

A reason for Chen's and Polster's lower total multiplicity is that these data were normalized to the annihilations. Lubinski *et al.* [16] found that in antiproton annihilation with ^{238}U 11.4% of the residual nuclei have mass number (A-1). Hence at least 11.4% of the annihilations result neither in fission nor in nucleon emission from the residual nuclei. Therefore the results of Polster and Chen have to be multiplied by a factor of $100/(100-11.4)=1.13$ to be compared with ours, strongly improving the agreement for the total neutron multiplicity.

A. Other methods in $\bar{p}$-induced fission

Measuring precisely the mass loss gives another possibility to directly determine the number of nucleons lost during a high-energy fission reaction. Moreover, the strong correlation between the mass of a fissioning nucleus and the TKE of this nucleus allows to estimate the number of pre- and postscission nucleons. The correlation between TKE and mass in fission is due to the fact that the TKE determining Coulomb energy of the fragments depends mainly on the radius of the fragments. Viola *et al.* [17] give an empirical formula describing this behavior.

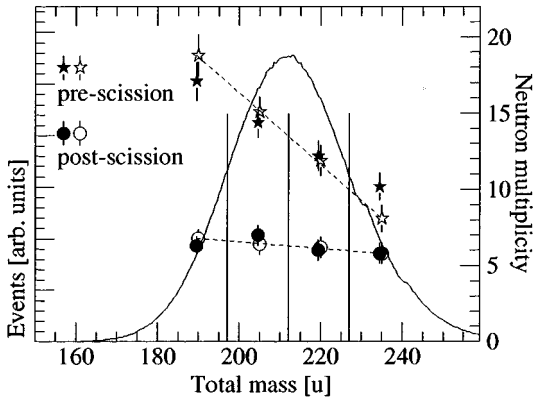

FIG. 8. Distribution of the sum of the two fragment masses $m_{FF1}+m_{FF2}$ for the reaction ^{238}U($\bar{p},f$). The three vertical lines separate the four mass-loss windows set on the mass distribution. The filled data points show the pre- and postscission multiplicity as a function of total mass and without correction for mass resolution. The open data points show the respective multiplicities M corrected for mass resolution. Due to the averaging properties of the mass-resolution correction the open data points are on straight lines (indicated by dashed lines).

TABLE VII. Results of inclusive experiments on $\bar{p}$ annihilation at ^{238}U. The neutron multiplicities M in the first two rows are normalized to the number of the annihilations. Multiplying the multiplicities in columns 2 and 3 by a factor of 1.13 yields numbers per fission. The multiplicities in the last column (this experiment) are normalized to the number of fission events.

Ref.	[15]	[14]	This experiment	
M_{INC}	4.49(75)	3.16(31)	3.33(30)	
M_{PE}	3.40(35)	1.15(21)	3.95(36)	
M_{EV}	8.42(25)	13.8(13)	13.2(11)	
M_{Σ}	16.3(9)	18.1(14)	20.4(12)	
T_{INC}	99.6(111)	37.7(25)	40.1(34)	MeV
T_{PE}	18.9(20)	5.78(79)	7.54(45)	MeV
T_{EV}	2.18(20)	2.67(20)	2.55(16)	MeV

The idea to deduce pre- and postscission multiplicity by TKE mass correlations was first worked out by Chestnov *et al.* [18] for 1 GeV-proton induced fission. Kim [19] used this method to estimate the number of pre- and postscission nucleons in $\bar{p}$-induced fission of ^{238}U. Their result strongly favors a quick transition to the scission point; more postscission nucleons (15(1)) are emitted than prescission nucleons 10(1) (see Table VIII). On the contrary, we found a much higher number of prescission neutrons than postscission neutrons. Emission of protons and complex charged particles would increase preferably our prescission value and even increase the discrepancy.

Chen *et al.* [15] measured already earlier pre- and postscission neutron multiplicities of $\bar{p}$-induced fission of ^{238}U, but they give only total multiplicities per annihilation

TABLE VIII. Comparison of measured pre- and postscission multiplicities for nucleons and neutrons. In the first row the first number in a column gives the number of nucleons with error; the number behind the error gives the estimated number of neutrons. The first number in each column of the second row (with error) gives the number of neutrons per annihilation. The second number (behind the error) gives the value per fission after applying a correction factor of 1.13.

Method	M_{pre}	M_{post}	Ref.
Spectroscopy of fragment masses: m_{tot}-TKE correlation	10(1) 8.0	15(1) 14.5	[19]
Neutron counting: three-source-fit	7.89(83) 8.9	8.42(25) 9.5	[15]
Neutron counting: Moving-source parametrization	13.6(8)	6.3(6)	

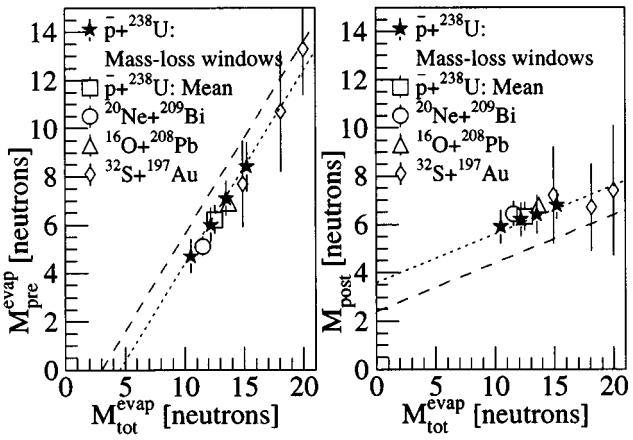

FIG. 9. Systematics of $M_{\rm pre}^{\rm evap}$ and $M_{\rm post}$: Evaporative pre- $M_{\rm pre}^{\rm evap}$ and postscission $M_{\rm post}$ neutron multiplicities as a function of the total number of evaporated neutrons $M_{\rm tot}^{\rm evap}$. The dashed lines are according to the empirical formulas of Hilscher *et al.* [20]. The dotted lines follow a linear dependence with the same slope but with a different offset parameter of $M_0=4.5$ (dashed lines: $M_0=3.0$). The references for the heavy-ion experiments are given in Table IX.

and not per fission event. Like their total multiplicity value in Sec. IV we corrected their pre- and postscission multiplicity by a factor of 1.13. Then we get 8.9 and 9.5 for the pre- and postscission neutron number, respectively. Chen *et al.* did not use the pulse-shape discrimination technique for selecting neutrons against γ's, their high value for the T parameters of 99.6 MeV and 18.9 MeV and the total absence of evaporation from the compound nucleus indicates that the large value of postscission neutrons includes a part of the compound-nucleus evaporation. Physically it cannot be expected that the emission of neutrons switches suddenly from the high-energy prescission emission to the emission of moderate-energy neutrons from the fragments.

B. Heavy ion and stopped $\bar{p}$-induced fission

For fission induced by heavy ions a large set of data exists in the excitation-energy region of 100–500 MeV. The main result of the heavy-ion induced fission experiments is a nearly constant number of postscission neutrons as a function of excitation energy while the evaporative prescission multiplicity increases strongly with excitation energy. The same behavior was found for the neutron multiplicities after $\bar{p}$-induced fission. The gain in the total neutron multiplicity appears to 80% in the increase of the number of prescission neutrons and only to 20% in the rise of the postscission neutron number. This is shown by the lines in Fig. 9, following a systematic approach given by Hilscher and Rossner [20] together with the experimental results of heavy-ion and $\bar{p}$-induced fission experiments (see Table IX). The lines in the picture represent the following formulas for the evaporative prescission and the postscission neutron multiplicity $M_{\rm pre}^{\rm evap}$ and $M_{\rm post}$, respectively,

$$M_{\rm pre}^{\rm evap}=0.8*(M_{\rm tot}^{\rm evap}-M_0),$$
$$M_{\rm post}=M_0+0.2*(M_{\rm tot}^{\rm evap}-M_0). \quad (6)$$

TABLE IX. Preequilibrium ($M_{\rm PE}$), evaporative prescission ($M_{\rm pre}^{\rm evap}$) and postscission ($M_{\rm post}$) neutron multiplicities from p-induced fission compared with heavy-ion induced fission. The thermal excitation energy E^* was taken from the references; for this experiment it is derived from the energy balance of Sec. V B.

Reaction	E^* MeV	$M_{\rm PE}$	$M_{\rm pre}^{\rm evap}$	$M_{\rm post}$	Ref.
^{20}Ne+^{209}Bi	120	0.55	5.12(40)	6.44(50)	[21]
^{16}O+^{208}Pb	187	0.87(15)	6.9(3)	6.8(3)	[12]
^{32}S+^{197}Au	201	3.0(3)	7.7(18)	7.2(20)	[13]
$\bar{p}$+^{238}U	160	4.1(4)	6.2(6)	6.3(6)	
^{32}S+^{197}Au	311	4.4(6)	10.7(25)	7.4(27)	[13]
^{32}S+^{197}Au	431	4.1(5)	13.3(19)	6.7(18)	[13]

$M_{\rm tot}^{\rm evap}$ denotes the total evaporative neutron multiplicity. M_0 is an offset parameter and is set to 3.0 for the dashed lines and to 4.5 for the dotted lines in Fig. 9 in a Z region of the compound nuclei of 86–91. Equations (6) describe the data better for $M_0=4.5$. Note that the slope of the lines is not changed. Furthermore the correction for the mass resolution does not change the ratio between the pre- and postscission multiplicities.

Despite the difference in angular momentum of the compound nuclei formed in heavy-ion and in stopped-$\bar{p}$ induced fission, reactions with comparable excitation energies, the pre- and postscission neutron numbers for both reactions reveal a picture of slow fission compared with neutron and light charged particle emission. In both cases the increase in excitation energy goes mainly into cascade emission of nucleons and prescission evaporation. Regardless of the initial excitation energy the nucleus is relatively cold at the moment of scission and cannot benefit from the high energy initially transferred.

C. Fission induced by energetic protons

Considering the low angular-momentum transfer the high-energy proton-induced fission has more similarities with the $\bar{p}$-induced fission than the heavy-ion reactions. Unfortunately experimental data in a comparable excitation-energy region are scarce. With 1-GeV protons on ^{238}U, Chestnov *et al.* [18] undertook a measurement of the fission-fragment masses and derived, by exploiting the correlation between TKE and total fragment mass, the pre- and postscission nucleon number. Their results of 80% postscission emission of all emitted nucleons are in contradiction with ours and with those from heavy-ion experiments. The measurement of Kim [19] with a very similar technique tend to a high postscission nucleon number, too. The difference is probably connected to the method, because most of the heavy-ion data are the result of neutron anisotropy measurements.

Fraenkel *et al.* [22] measured the pre- and postscission neutrons from 475 MeV proton-induced fission of ^{238}U with the neutron counting technique and determined multiplicities by an iteration method. They got a number of 8.4(17) prescission and 8.6(17) postscission neutrons, not far from our results.

TABLE X. Comparison of the measured neutron multiplicities M with those calculated according to the statistical model without and with dynamical effects. The dynamical effects were taken into account in two ways: the third column (SSC) includes a finite saddle-to-scission transition time of 10^{-20} s. The last column is calculated following the approach of Kramers [31], introducing a viscosity of nuclear matter ($\gamma=0.7$).

	Experiment	No effects	Theory SSC	Theory with viscosity
M_{INC}	3.3(3)	3.13	2.90	3.06
M_{CN}	6.2(6)	1.74	6.84	7.00
M_{FF}	3.2(3)	7.11	3.57	3.75

V. DISCUSSION

A. The statistical model and dissipative effects

The formation of highly excited nuclei can be described by the intranuclear-cascade model. In the case of antiproton-induced reactions this approach is very successful and has led to a thorough understanding [23,24] of the antiproton nucleus interaction. This is not true for the deexcitation of a heavy nucleus, especially in the competition between fission and particle evaporation. The measurement of pre- and postscission neutron multiplicities is a good way to test this competition and is closely related to the dynamics of the fission process.

The standard method of describing high-energy fission is [25], following an idea of Bohr and Wheeler, the statistical model. They were able to derive a formula for the partial decay widths Γ_n for neutron emission and Γ_f for fission, respectively,

$$\frac{\Gamma_f}{\Gamma_n}=\frac{K_0 a_n(2\sqrt{a_n(E^*-B_f)}-1)}{4a^{2/3}a_f(E^*-B_n)}\exp(2\sqrt{a_f(E^*-B_f)} - 2\sqrt{a_n(E^*-B_n)}), \quad (7)$$

where B_n and B_f are the binding energy of a neutron and the fission-barrier height, respectively, a_n and a_f the level-density parameter for neutron emission and fission, K_0 and a are constants, and E^* is the excitation energy. It is a well-known fact [26–28] that the statistical model underestimates the ratio of pre- to postscission neutrons remarkably. Hence our model includes two effects influencing the dynamics of fission: (i) the prolonged transition time τ_{SSC} from saddle to scission point, and (ii) the viscosity γ of nuclear matter which delays the formation of the fissioning nucleus, and leads to an increase in Γ_f: $\Gamma_f^{\mathrm{vis}}=\Gamma_f(\sqrt{1+\gamma^2}-\gamma)$.

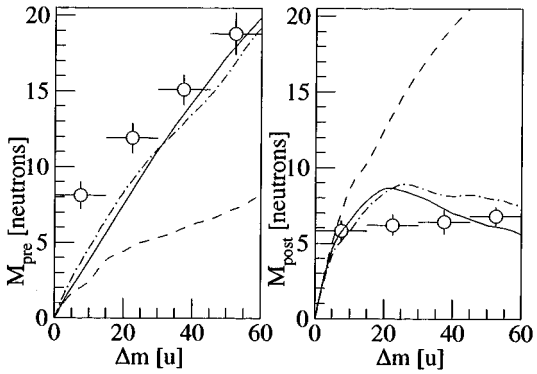

FIG. 10. Comparison of calculated pre- and postscission neutron multiplicities (curves) with the measured multiplicities (data points) as a function of mass loss. The dashed curve is calculated with the statistical model without dynamical effects. The dashed-dotted curve stands for a calculation taking into account the viscosity following the approach by Kramers [31] ($\gamma=0.7$). The solid curve is calculated with the assumption of a finite saddle-to-scission transient time $\tau_{\mathrm{SSC}}=10^{-20}$ s. For all calculations $a_f/a_n=1.02$ for $A>220$. For $A<220$ the ratio $a_f/a_n=1.08$ for the dashed-dotted line, and 1.02 for the standard calculation and the calculation with saddle-to-scission effects.

The importance of these effects were already pointed out by Grangé and Weidenmüller [29]. The general features of the cascade evaporation model we used are described in Ref. [11]. The level-density parameters a_f and a_n were obtained by fitting a large set of experimental data [30] at excitation energies up to about 100 MeV.

We tried three versions of the statistical-model calculation to be compared with the experimental results. The standard statistical model without any dynamical effects underestimates, especially for higher excitation energy (mass loss), the prescission neutron number (dashed line in Fig. 10, left side). This corresponds to a strongly increased number of post-scission neutrons M_{post}, as is shown by the dashed lines in Fig. 10 (right side). Taking into account either the viscosity of nuclear matter at the saddle point or the increase in the saddle-to-scission transient time in our calculation we have good agreement with the experimental results. This is demonstrated in Tables X and XI.

TABLE XI. Neutron multiplicities M calculated with the statistical model with dynamical effects. The mass-loss-corrected measured neutron multiplicities of Table VI are given in square brackets. M_{PE} for the calculation is included in M_{INC}.

Mass loss [u]	>45	30–45	15–30	<15
M_{INC}	5.4 [4.6]	3.9 [3.6]	2.7 [2.8]	1.3 [1.8]
M_{PE}	– [5.8]	– [4.4]	– [3.1]	– [1.6]
M_{CN}	11.2 [8.4]	8.7 [7.1]	6.3 [6.0]	3.4 [4.7]
$M_{\mathrm{FF1,2}}$	4.1 [3.4]	4.1 [3.2]	4.3 [3.1]	2.7 [2.9]
M_{pre}	16.6 [18.8]	12.6 [15.1]	9.0 [11.9]	4.6 [8.1]
M_{post}	8.2 [6.8]	8.3 [6.4]	8.5 [6.2]	5.5 [5.8]
M_{Σ}	24.8 [25.6]	20.9 [21.5]	17.5 [18.1]	10.1 [13.9]

B. Energy-balance considerations

Combining the charged-particle multiplicities and mean energies from earlier experiments [14,32,33] with our neutron multiplicities one can determine the excitation energy during the different stages of deexcitation. The total energy E which is required to emit different kinds of particles j with a mean energy $\langle E_j \rangle$ and a multiplicity M_j is given by

$$E = \sum_{j=n,p,d} M_j(\langle E_j \rangle + B_j) = \sum_{j=n,p,d} M_j(\tfrac{3}{2}T_j + B_j), \quad (8)$$

where B_j is the separation energy of the emitted particle. The mean energy can be calculated from the fitted temperature parameters and is for the distributions given by $\langle E_j \rangle = 3/2T_j$. The separation energy is about 8 MeV for neutrons and protons. For the deuteron separation energy we took the sum of the nucleon separation energies. The emission of t, ^{4}He, and complex particles was not taken into account because of their low multiplicities [32,33]. The proton multiplicity of 1.04 measured by Polster *et al.* [14], which was determined by extrapolation from proton energies above 30 MeV to energies up to the Coulomb barrier indicates that only protons with energies higher than the Coulomb barrier of uranium (15.3 MeV) could be emitted. Markiel *et al.* [32] found that 0.3 protons are emitted with energies below 12 MeV, which is only possible as evaporation from the fragments with a Coulomb barrier of about 10 MeV. The emission of γ's was measured by Armstrong *et al.* [34]. They found on the average two γ's with an energy of 6 MeV per fission event.

The uncertainty of the energies estimated in such a way is about 10% following from the errors of multiplicities and T parameters. Applying Eq. (8) yields the energy balance

$\Delta E^n_{\rm INC} =$	$3.3(\frac{3}{2}40.1+8) =$	225 MeV
$\Delta E^p_{\rm INC} =$	$1.04(\frac{3}{2}37.7+8) =$	67 MeV
$\Delta E^d_{\rm INC} =$	$0.14(\frac{3}{2}22.6+16) =$	7 MeV
$\Delta E_{\rm INC} =$		299 MeV
$\Delta E^n_{\rm PE} =$	$4.1(\frac{3}{2}7.54+8) =$	78 MeV
$\Delta E^n_{\rm CN} =$	$6.2(\frac{3}{2}2.58+8) =$	73 MeV
$\Delta E^n_{\rm FF} =$	$6.3(\frac{3}{2}1.9+8) =$	68 MeV
$\Delta E^p_{\rm FF} =$	$0.3(12+8) =$	6 MeV
$\Delta E_\gamma =$	$2\times 6 =$	12 MeV
$\Delta E_{\rm total} =$		536 MeV

The derived total transferred energy $\Delta E_{\rm total}$ of about 540(50) MeV is somewhat larger than the value of 490 MeV derived by Polster *et al.* [14]. This comes mainly from our higher pre-equilibrium multiplicity. Anyhow one should keep in mind that the fission events following annihilation are a special subset of the annihilation events.

The mass of the fissioning nucleus itself can be estimated by the mass and charged particle loss during the intranuclear cascade. The mean mass loss amounts to 4–5 mass units, the mean charge loss to 1–2 charge units. Thus the nuclei ^{233}Th or ^{233}Pa are a good estimate for the average fissioning nucleus.

The thermal excitation energy follows from this energy balance as the sum of the energies of compound-nucleus and fission-fragment evaporation particles and amounts to about 160(16)MeV $(\Delta E^n_{\rm CN} + \Delta E^n_{\rm FF} + \Delta E^p_{\rm FF} + \Delta E_\gamma)$, as derived from the energy balance. For the initial excitation energy of the fissioning nucleus (^{233}Pa, ^{233}Th) we have to subtract the effective fission Q value $Q_{\rm eff} = Q_{\rm fis} - {\rm TKE} \sim 20$ MeV resulting in 140 MeV excitation energy. Similarly the thermal excitation energy of the fragments is 86(9)MeV $(\Delta E^n_{\rm FF} + \Delta E^p_{\rm FF} + \Delta E_\gamma)$. This confirms that the nucleus is relatively cold at the moment of scission and more than 2/3 of the transferred energy is lost before the nucleus attains thermodynamic equilibrium. The thermal excitation energies can be also estimated with a simple formula from the statistical model and the knowledge of the mean temperature T of the nucleus

$$E^* = a^* T^2. \quad (9)$$

Here a is the level-density parameter, which can be calculated from the mass number A of the nucleus: $a = A/10$ [1/MeV]. T is the temperature parameter. From this approach an excitation energy of the fragments of 76(14) MeV can be derived. For the compound nucleus this energy is 140(23) MeV according to Eq. (9). The somewhat lower compound-nucleus excitation energy which agrees within the errors with the value given above is an indication of dissipative effects during saddle to scission transition setting free additional excitation energy which appears in the multiplicity and mean energy based on an estimate of energy of 160(16) MeV above.

VI. CONCLUSIONS

Antiproton induced fission at high excitation energies is unique in the sense that during formation of the compound nucleus little rotation, compression and collective distortion is introduced to the fissioning nucleus. Such distortions could have drastic effects on the dynamics of fission. Consequently it is important to verify whether nuclei produced in this way exhibit a similar slow fission dynamics as found for a large variety of heavy-ion induced reactions, that is with a completely different formation dynamics. This was particularly needed since previous measurements [19,35] had indicated by an indirect method that antiproton induced fission might be considerably faster than heavy-ion induced fission. By exploiting the number of neutrons emitted prior and post to scission we have shown that antiproton induced fission perfectly complements and corroborates the findings with heavy ions: most of the excitation energy is emitted prior to scission indicative for a long prescission time.

ACKNOWLEDGMENTS

We wish to thank the LEAR and PS staffs at CERN for providing an excellent antiproton beam, and K. Nacke and Dr. Maier-Komor for the target. For technical and electronics support we thank H. Hagn. For help during the experiment we thank A. Grabowska, J. Jastrzebski, W. Kurcewicz, P. Lubinski, and A. Trzcinska. Two of us (H.M. and H.S.P.) acknowledge support by a NATO Office of Scientific Affairs Grant. We express our gratitude to the team of experiment PS205 at LEAR for the possibility to use the data-acquisition system EXP.

[1] Y.S. Kim, P. Hofmann, H. Daniel, T. von Egidy, T. Haninger, F.J. Hartmann, M.S. Lotfranaei, and H. Plendl, Nucl. Instrum. Methods Phys. Res. A **329**, 403 (1993).
[2] F.J. Lynch, IEEE Trans. Nucl. Sci. **NS-22**, 58 (1975).
[3] R.A. Cecil, B.D. Anderson, and R. Madey, Nucl. Instrum. Methods **161**, 439 (1979).
[4] H.W. Schmitt, W.E. Kiker, and C.W. Williams, Phys. Rev. **137**, B837 (1965).
[5] H.-O. Neidel and H. Henschel, Nucl. Instrum. Methods **178**, 137 (1980).
[6] W. Schmid, Jahresbericht 1994 des Beschleunigerlaboratoriums der Universität und der Technischen Universität München, p. 109.
[7] W. Schmid, Ph.D. Thesis, Technische Universität München, 1996.
[8] L.C. Northcliffe and R.F. Schilling, Nucl. Data, Sec. A **7**, 233 (1970).
[9] D. Hilscher, J.R. Birkelund, A.D. Hoover, W.U. Schröder, W.W. Wilke, J.R. Huizenga, A.C. Mignerey, K.L. Wolf, H.F. Breuer, and V.E. Viola, Phys. Rev. C **20**, 576 (1979).
[10] G.N. Harding and F.J.M. Farley, Proc. Phys. Soc. London, Sec. A **69**, 853 (1956).
[11] P. Hofmann, A.S. Iljinov, Y.S. Kim, M.V. Mebel, H. Daniel, P. David, T. von Egidy, T. Haninger, F.J. Hartmann, J. Jastrzebski, W. Kurcewicz, J. Lieb, H. Machner, H.S. Plendl, G. Riepe, B. Wright, and K. Ziock, Phys. Rev. C **49**, 2555 (1994).
[12] D.J. Hinde, D. Hilscher, H. Rossner, B. Gebauer, M. Lehmann, and M. Wilpert, Phys. Rev. C **45**, 1229 (1992).
[13] E. Mordhorst, M. Strecker, H. Frobeen, M. Gasthuber, W. Scobel, B. Gebauer, D. Hilscher, M. Lehmann, H. Rossner, and Th. Wilpert, Phys. Rev. C **43**, 716 (1991).
[14] D. Polster, D. Hilscher, H. Rossner, T. von Egidy, F.J. Hartmann, J. Hoffmann, W. Schmid, I.A. Pshenichnov, A.S. Iljinov, Ye.S. Golubeva, H. Machner, H.S. Plendl, A. Grochulska, J. Jastrzebski, W. Kurcewicz, P. Lubinski, J. Eades, and S. Neumaier, Phys. Rev. C **51**, 1167 (1995).
[15] B. Chen, T.A. Armstrong, R.A. Lewis, R. Newton, G.A. Smith, J.P. Boquet, F. Malek, H. Nifenecker, M. Maurel, M. Maurel, E. Monnand, P. Perrin, C. Ristori, G. Ericsson, T. Johansson, G. Tibell, M. Rey-Campagnolle, S. Polikanov, T. Krogulski, and J. Mougey, Phys. Rev. C **45**, 2332 (1992).
[16] P. Lubiński, J. Jastrzebski, A. Grochulska, A. Stolarz, A. Trzcińska, W. Kurcewicz, F.J. Hartmann, W. Schmid, T. von Egidy, J. Skalski, R. Smolańczuk, S. Wycech, D. Hilscher, D. Polster, and H. Rossner, Phys. Rev. Lett. **73**, 3199 (1994).
[17] V.E. Viola, K. Kwiatkowski, and M. Walter, Phys. Rev. C **31**, 1550 (1985).
[18] Yu.A. Chestnov, A.V. Kravtsov, B.Yu. Sokolovskii, and G.E. Solyakin, Yad. Fiz. **45**, 19 (1987) [Sov. J. Nucl. Phys. **45**, 11 (1987)].
[19] Y.S. Kim, Ph.D. Thesis, Technische Universität München, 1992.
[20] D. Hilscher and H. Rossner, Ann. Phys. (Paris) **17**, 471 (1992).
[21] D.J. Hinde, H. Ogata, M. Tanaka, T. Shimoda, N. Takahashi, A. Shinokara, S. Wakamatsu, and H. Okamura, Phys. Rev. C **39**, 2268 (1989).
[22] Z. Fraenkel, A. Breskin, R. Chechik, S. Wald, R. Abegg, H.W. Fielding, P. Kitching, S.T. Lam, G.C. Neilson, W.C. Olsen, and J. Uegaki, Phys. Rev. C **41**, 1050 (1990).
[23] A.S. Iljinov, V.I. Nazaruk, and S.E. Chigrinov, Nucl. Phys. **A382**, 378 (1982).
[24] J. Cugnon and J. Vandermeulen, Nucl. Phys. **A445**, 717 (1985).
[25] J.O. Newton, Fiz. Elem. Chas. At. Yad. **21**, 821 (1990) [Sov. J. Part. Nucl. **21**, 349 (1990)].
[26] E. Holub, D. Hilscher, G. Ingold, U. Jahnke, H. Orf, and H. Rossner, Phys. Rev. C **28**, 252 (1983).
[27] D.J. Hinde, R.J. Charity, G.S. Foote, J.R. Leigh, J.O. Newton, S. Ogaza, and A. Chattejee, Nucl. Phys. **A452**, 550 (1986).
[28] A. Gavron, A. Gayer, J. Boissevain, H.C. Britt, T.C. Awes, J.R. Beene, B. Cheynis, D. Drain, R.L. Ferguson, F.E. Obenshain, F. Plasil, G.R. Young, G.A. Petitt, and C. Butler, Phys. Rev. C **35**, 579 (1987).
[29] P. Grangé and E. Weidenmüller, Phys. Rev. C **27**, 2063 (1983).
[30] A.S. Iljinov, M.V. Mebel, N. Bianchi, E. de Sanctis, C. Guaraldo, V. Lucherini, V. Muccifora, E. Polli, A.R. Reolon, and P. Rossi, Nucl. Phys. **A543**, 517 (1992).
[31] H.A. Kramers, Physica (Amsterdam) **7**, 284 (1940).
[32] W. Markiel, H. Daniel, T. von Egidy, F.J. Hartmann, P. Hofmann, W. Kanert, H.S. Plendl, K. Ziock, R. Marshall, H. Machner, G. Riepe, and J.J. Reidy, Nucl. Phys. **A485**, 445 (1988).
[33] P. Hofmann, F.J. Hartmann, H. Daniel, T. von Egidy, W. Kanert, W. Markiel, H.S. Plendl, H. Machner, G. Riepe, D. Protic, K. Ziock, R. Marshall, and J.J. Reidy, Nucl. Phys. **A512**, 669 (1990).
[34] T.A. Armstrong, R. Bishop, V. Harris, R.A. Lewis, E.D. Minor, and G.A. Smith, Z. Phys. A **331**, 519 (1988).
[35] Y.S. Kim, A.S. Iljinov, M.V. Mebel, P. Hofmann, H. Daniel, T. von Egidy, T. Haninger, F.J. Hartmann, H. Machner, H.S. Plendl, and G. Riepe, Phys. Rev. C **54**, 2469 (1996).